Vol 18 No 6, June 2009
1674-1056/2009/18(06)/2452-07

Chinese Physics B

© 2009 Chin. Phys. Soc.
and IOP Publishing Ltd

Three-dimensional simulation of a Ka-band relativistic Cherenkov source with metal photonic-band-gap structures*

Gao Xi(高 喜)[a)†], Yang Zi-Qiang(杨梓强)[a)], Qi Li-Mei(亓丽梅)[a)], Lan Feng(兰 峰)[a)], Shi Zong-Jun(史宗君)[a)], Li Da-Zhi(李大治)[b)], and Liang Zheng(梁 正)[a)]

[a)] *Research Institute of High Energy Electronics, University of Electronic Science and Technology of China, Chengdu* 610054, *China*

[b)] *Institute for Laser Technology, 2-6 Yamada-Oka, Suita, Osaka* 565-0871, *Japan*

(Received 6 October 2008; revised manuscript received 21 December 2008)

This paper presents a three-dimensional particle-in-cell (PIC) simulation of a Ka-band relativistic Cherenkov source with a slow wave structure (SWS) consisting of metal photonic band gap (PBG) structures. In the simulation, a perfect match layer boundary is employed to absorb passing band modes supported by the PBG lattice with an artificial metal boundary. The simulated axial field distributions in the cross section and surface of the SWS demonstrate that the device operates in the vicinity of the π point of a TM_{01}-like mode. The Fourier transformation spectra of the axial fields as functions of time and space show that only a single frequency appears at 36.27 GHz, which is in good agreement with that of the intersection of the dispersion curve with the slow space charge wave generated on the beam. The simulation results demonstrate that the SWS has good mode selectivity.

Keywords: Cherenkov source, slow wave structure, photonic band gap, three-dimensional particle-in-cell

PACC: 5420M

1. Introduction

Vacuum electron devices are important sources of high-power microwaves for use in industrial heating, radar, communications, and many other applications. Extension of the operation frequency of the sources to higher values is of great interest and would open up many new applications. As the operation frequency increases to the millimeter-wave range, the output power must be limited as the dimensions are too small. An overmoded structure can alleviate the problem, but mode competition is another difficult problem to be solved.[1−4]

In recent years, many theoretic and experimental studies of PBG structures have demonstrated that they can effectively depress mode competition in vacuum electron devices in microwave and millimeter wave ranges. For example, they have been successfully employed in accelerators,[5] gyrotrons,[6] reflex klystrons[7] and traveling wave tubes[8,9] to depress the unwanted modes.

In Cherenkov generators, PBG structures have also been proposed to construct SWS to reduce mode competition.[10−12] However, to our knowledge, there are no research papers reporting the radiation characteristics of PBG SWS with an electron beam.

In this paper, with the help of three-dimensional (3D) PIC simulation, we study the physical process between space charge and electromagnetic field in the SWS proposed in Ref.[12]. This simulation is carried out first, from which we can observe the radiation characteristics and mode selectivity of the SWS.

This paper is organized as follows: Section 2 contains the dispersion characteristics of SWS and the analysis of the Q factor of the PBG cavity; the physical model of PIC simulation is described in Section 3; the simulation results and discussions are given in Section 4, and the conclusion is given in Section 5.

*Project supported by the National Key Basic Research Program of China (Grant No 2007CB31040) and the National Natural Science Foundation of China (Grant No 60571020).

†E-mail: gaoxi_2594@yahoo.cn

2. The dispersion characteristics of SWS and the Q factor of the PBG cavity

The SWS with PBG structures is shown in Fig.1. The parameters of the SWS and PBG structures are the same as those given in Ref.[12] and shown in Table 1. Figure 2 shows the dispersion characteristics of the SWS. One can see from this figure that the electronic field of the intersection of the dispersion curve with the electron beam is completely occupied by slow waves, which makes the electric fields concentrate near the surface of the SWS.

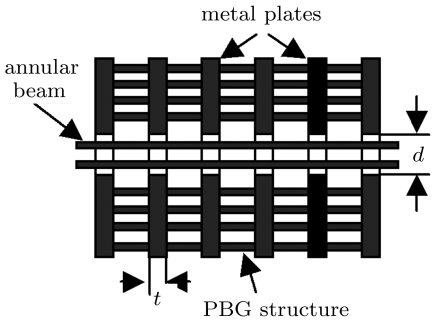


Fig.1. The high frequency system with PBG structure.

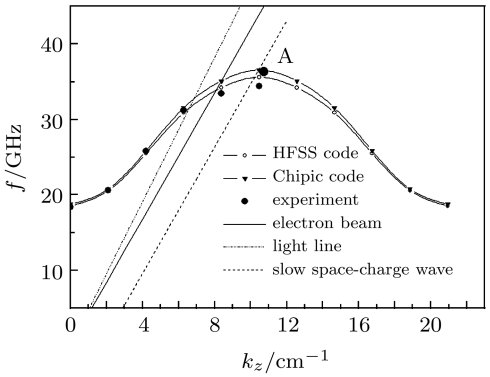


Fig.2. The dispersion curve of SWS.

Table 1. Parameters of PBG structures and SWS.

rod radius	$r = 0.5$ mm
spacing between the rods	$a = 3.8$ mm
metal plate inner radius	$d/2 = 5.8$ mm
metal plate thickness	$t = 2.0$ mm
SWS periodic length	$l = 3.0$ mm

In addition, with the help of a high frequency structure simulator (HFSS), the Q factor of PBG cavity that depends on the number of layers of metal rods is studied. In order to obtain the relation, a PBG cavity with an open boundary should be constructed. So the outer metal wall is replaced by an absorber such as a perfectly matched layer (PML) to absorb electromagnetic waves leaking out of the transverse of the PBG structure.[13] The Q factor can be obtained by calculating the resonant frequency of the TM_{01}-like mode of the cavity (see Fig.3). Figure 4 shows the variation of Q factor with the number of layers of metal rods (denoted by N). It is found that even though there are only two layers of metal rods, the Q factor is still over 5000. This phenomenon indicates that the electromagnetic energy of the defect mode is mainly confined by the first few rows of rods closest to the defect, especially the innermost two rows of metal rods.

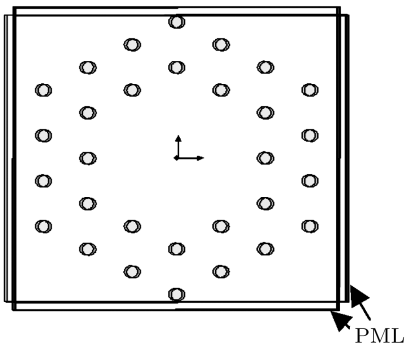


Fig.3. The physical model for computing the Q factor of the PBG cavity using HFSS code.

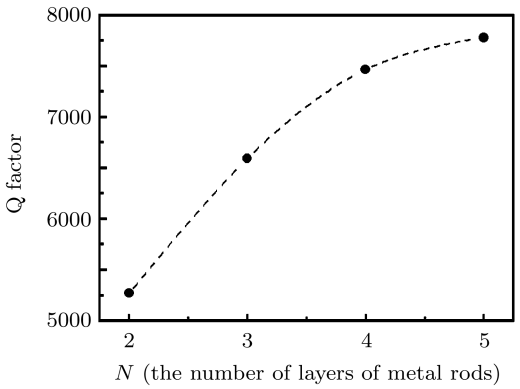


Fig.4. Q factor dependence on the number of layers of metallic rods.

3. Description of PIC simulation

According to Ref.[12], any modes above the TM_{02}-like mode are not confined within the defect. But these modes are supported by the lattice and strongly affect the electron beam when an artificial metallic boundary is used in the PIC simulation. In

order to eliminate these higher modes, the metallic boundary is replaced by absorbers. Simultaneously, the PBG structure is made up of two layers of metal rods. Reducing the number of layers of metal rods will affect the operating mode very little, while significantly decreasing the Q factor of higher order modes because the operation mode is primarily confined by the innermost two rows of metal rods and the higher order modes exist within the entire lattice. A simulation of the PBG cavity with three rows of rods replaced by two rows of rods reduces the Q factor of the TM_{01}-like mode from 6600 to 5270, while reducing the Q value of the TM_{02}-like mode from 2370 to 270. However, reducing the metal rods to two rows can greatly save simulation time. Figure 5 shows the 3D physical mode for the PIC simulation. An annular electron beam is generated from a cathode located at the left end and confined by an axial magnetic field to run along the z-axis. The electron beam parameters for the simulation are shown in Table 2.

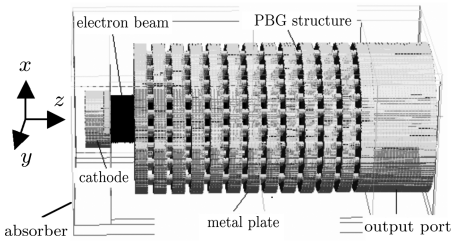


Fig.5. The 3D physical model for the simulation.

As for the diagnostics, 3D simulation software using Chipic code[14] allows us to observe a variety of physical quantities such as operation mode, electromagnetic field (as functions of time and space), power outflow, current (as a function of space), and electron phase-space trajectories.

Table 2. The electron beam parameters for the simulation.

beam thickness	$\sigma = 1.0$ mm
beam-SWS distance	$\delta = 1$ mm
beam voltage	$V = 550$ kV
beam current	$I = 2$ kA
external magnetic field	$B_z = 4.0$ T
period number	$N' = 12$

4. Simulation results and discussion

Figure 6(a) shows the electric field patterns of the operation mode observed in the simulation; Figure 6(b) displays the electric field profile of the π-mode of the TM_{01}-like mode in the cold cavity calculated using HFSS code. Comparing Figs.6(a) and 6(b), one can deduce that the operation mode of the device is a TM_{01}-like mode in the vicinity of the π-mode. On the other hand, we note that there are some electric fields outside the PBG structure in Fig.6(a). They may consist of the following two parts: one is the electromagnetic energy of the operation mode leaking out from the transverse of the PBG cells due to their finite Q factor; the other is the electromagnetic wave excited by the electron beam with frequency lying in the pass band, which just demonstrates the function of the mode selectivity of the PBG cells. Figure 7 shows the vectors of the E_z field on the surface of the SWS. The electric field in the neighboring cavity is inverted, which means that the device operates in the vicinity of the π-mode of the TM_{01}-like mode.

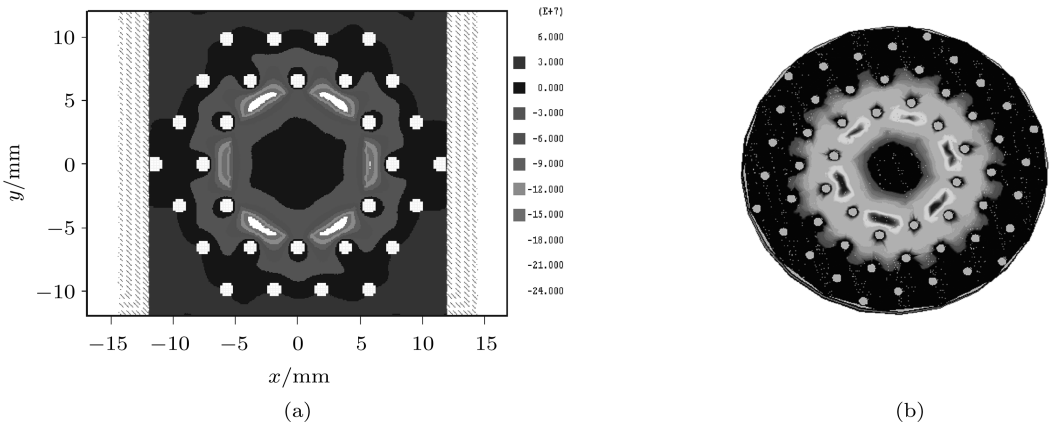


Fig.6. E_z field patterns in a cross section of SWS and the observing plane lying in the midst of two neighboring metal plates: (a) calculated using PIC simulation; (b) π-mode calculated using HFSS code.

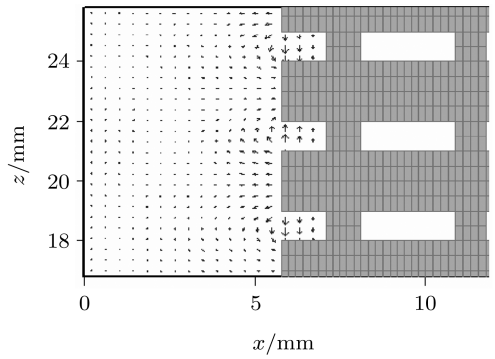


Fig.7. The vector plots of E_z field in the x–z plane.

Figure 8 shows the electronic kinetic energy as a function of space. Appreciable energy modulation and energy exchange between the beam and the electromagnetic wave is visible. In order to investigate this phenomenon in greater detail, we plot the beam current as a function of z at the times 4 ns and 10 ns respectively, as shown in Fig.9. At $t = 4$ ns, the bunching has a clear period twice that of the SWS, which again indicates that the device operates in the vicinity of the π-mode.[15] However, the current at $t = 10$ ns shows a great difference. The current curve becomes distorted after the position $z = 24.25$ mm because of the strong interaction between the electron beam and the electromagnetic wave.

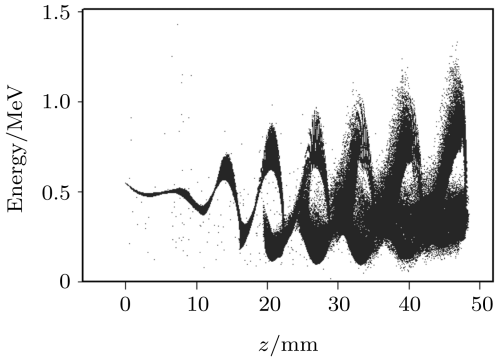


Fig.8. The energy of the electrons versus z at 19.93 ns.

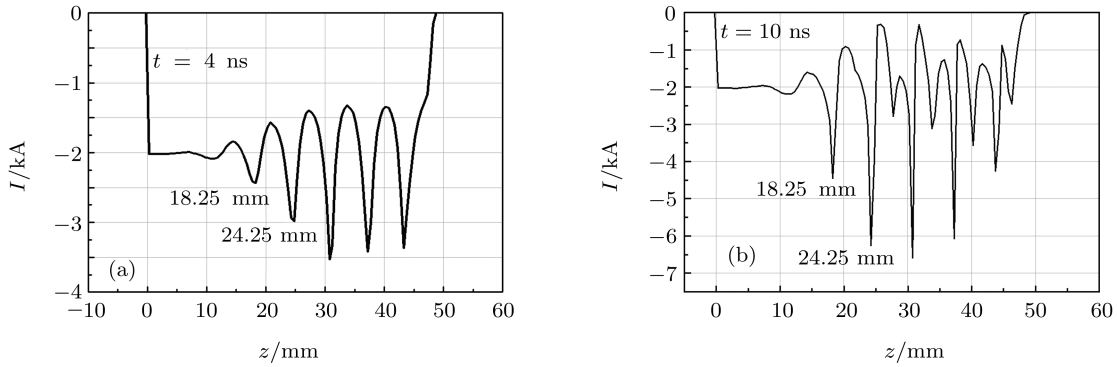


Fig.9. Current as a function of z at two different times.

According to the Floquet theorem, the z-dependence of the fields in our device can denote the form $\sum_{n=-\infty}^{\infty} E_{zn}(x,y)\mathrm{e}^{\mathrm{i}(k_n z-\omega t)}$, where $k_n = k_z + nk_0$. If a field variable is measured as a function of z for fixed x, y and t, the corresponding Fourier transform will present peaks at wave numbers $k_z + nk_0$, where n is the number of space harmonics and $k_0 = 2\pi/l$ (l is the periodic length of the SWS). Figure 10 shows the space dependence of the E_z field near the SWS and the corresponding fast Fonrier transform (FFT). In Fig.10(b), there are two peaks corresponding to wave numbers 10.217 and 31.571 cm^{-1}, which approximately satisfy the formula $k_n = k_z + nk_0$. However in Fig.2, for the case of $k_z = 10.217$ cm^{-1}, the corresponding frequency in the dispersion curve is 36.44 GHz which deviates from the frequency (35.32 GHz) of the intersection of the beam line with the dispersion curve. In fact, the operation point should be the intersection of the dispersion curve with the line of the slow space-charge wave generated from the electron beam. The slow space-charge wave is described as follows:[16]

$$\omega = kv_\mathrm{e} - \omega_\mathrm{p} = kv_\mathrm{e} - \left(\frac{I_\mathrm{e}e}{\varepsilon_0 m\pi r^2 v_\mathrm{e}}\right)^{1/2}, \tag{1}$$

where v_e is the beam velocity, ω_p is the plasma angular frequency of the beam given by $\omega_\mathrm{p} = \left(n_\mathrm{e}e^2/\varepsilon_0 m\right)^{1/2}$; n_e, e and m are the electron density, charge and mass, respectively. I_e is the beam current and r the beam radius.

The line of the slow space-charge wave determined by Eq.(1) is shown as a dashed line in Fig.2. Consequently, the frequency of the intersection of the slow space-charge wave with the dispersion curve is approximately equal to the frequency of $k_z = 10.217$ cm^{-1}.

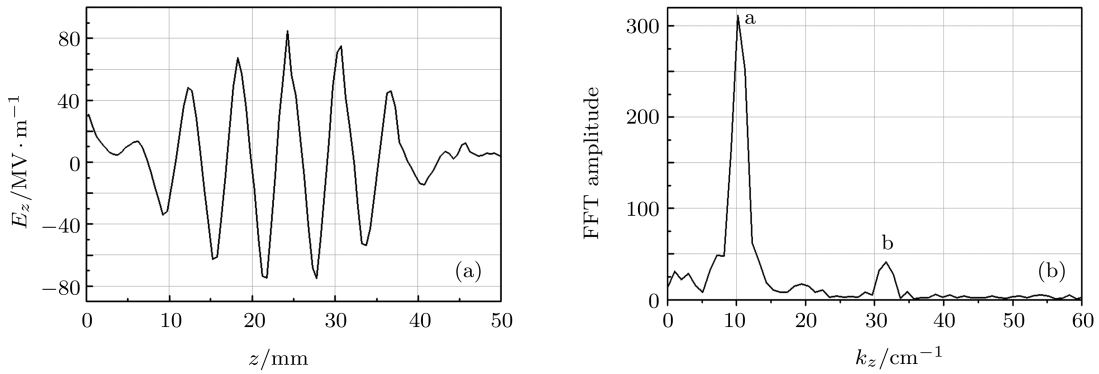


Fig.10. Space dependence of the electronic field: (a) $E_z(z)$ near SWS, (b) corresponding FFT.

The RF voltage on the surface of the SWS between the simulation times of 11.5 and 11.8 ns was observed and is presented in Fig.11(a) and the corresponding FFT spectrum is shown in Fig.11(b). From the FFT spectrum, the operation frequency is observed at 36.267 GHz. This is in agreement with the frequency of the intersection of the dispersion curve with the line of the slow space-charge wave in Fig.2. The frequency spectrum also shows that the operation frequency is single and the mode competition does not appear, which can be attributed to the mode selectivity of the PBG cells in the SWS.

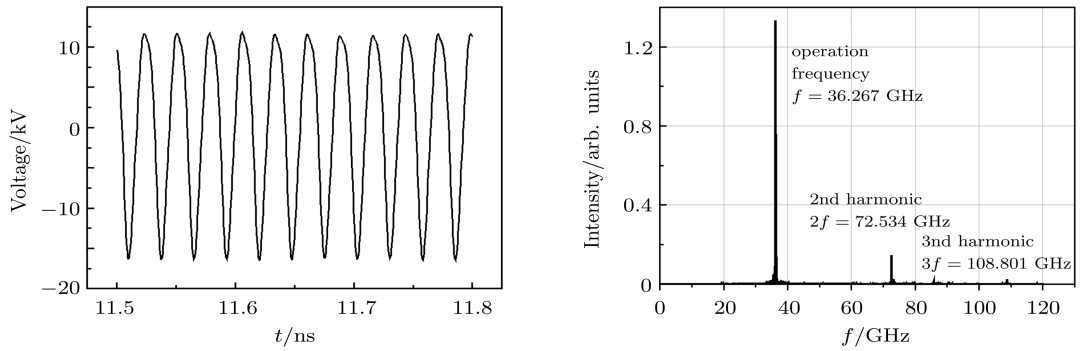


Fig.11. Induced voltage on the first-cavity of the SWS and corresponding FFT.

The efficiency of the device at different external magnetic fields is shown in Fig.12. When the electron beam is guided by a lower external magnetic field such as 1 T, the beam has poor quality so the device has very low efficiency. With the increase of external magnetic field, the beam's quality becomes better, which improves the efficiency. But when the external magnetic field keeps rising, a dip in efficiency appears at 6 T due to cyclotron absorption.

In a Cherenkov device, the synchronization condition should be satisfied

$$\omega \simeq k v_z, \tag{2}$$

and for some resonance value of the external axial magnetic field the cyclotron will be satisfied for the 1st spatial harmonic,[14]

$$\omega \simeq (k - k_0) v_z + \Omega_c, \tag{3}$$

where $\Omega_c = eB_0/mc\gamma$ is the relativistic cyclotron frequency. According to Eqs.(2) and (3), B_0 can be expressed as follows:

$$B_0 = \frac{2\pi}{l} \cdot \frac{mc\gamma}{e} v_z, \tag{4}$$

where l is the periodic length of the SWS, c is the velocity of light, and γ is a relativistic factor. If the external axial magnetic field equals B_0, the electron beam will absorb energy from the electromagnetic wave and decrease the efficiency of device. For the case of $V = 0.55$ MV, the corresponding magnetic field for cyclotron absorption is $B_0 = 6.48$ T which is in agreement with that obtained from the simulation. Figure 13 shows the output power integration of a time-averaged Poynting vector over the output end. The device begins to start at about 3 ns and reaches saturation at about 8 ns.

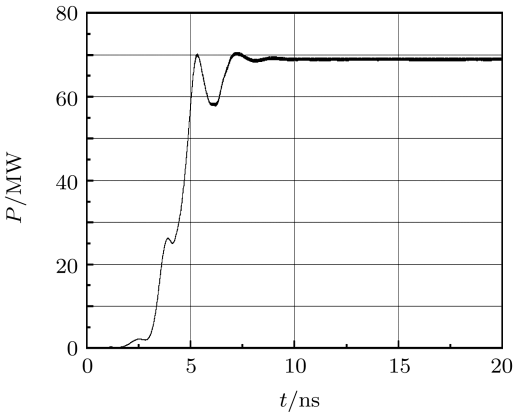


Fig.13. Time dependence of output power.

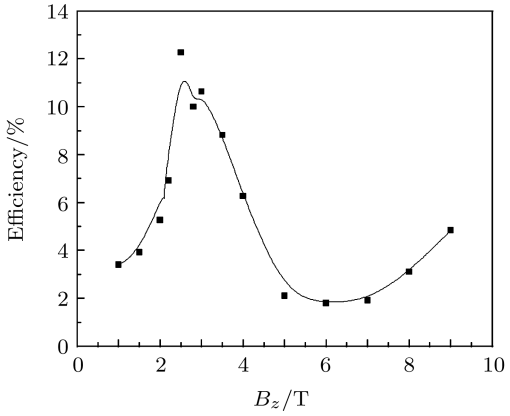


Fig.12. Efficiency of the device as a function of external magnetic field.

Based on the PIC simulation, an experiment with a relativistic electron beam (named hot-test) will be performed. Figure 14 shows the schematic of the experimental setup. The experiment will be carried out using a high-power pulsed source (LIA-2006) which can produce a relativistic electron beam with voltage and current above 400 kV and 1 kA, respectively. The generation of the annular electron beam and signal detection may be difficult problems that need to be solved in the experiment. The annular electron beam is generated by a coaxial cold electron gun[1] and the frequency will be measured by a dispersive delay line.[17]

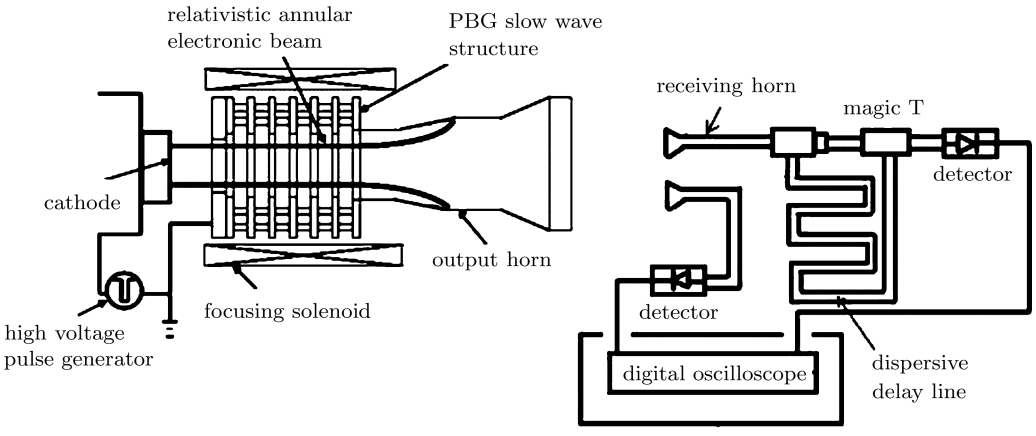


Fig.14. Schematic of the future hot test experiment.

5. Conclusion

A Ka band Cherenkov source with SWS consisting of metal PBG structures has been studied by using HFSS and 3D PIC simulation codes. The investigation of the Q factor of the PBG cavity showed that the electromagnetic energy of the defect mode is mainly confined by the innermost two layers of metal rods. The beam-wave interaction process in the SWS was analyzed by 3D PIC simulation. Space patterns of the E_z field in cross section and vector plots of the E_z field on the surface of the SWS are given. It is demonstrated that the operation mode is in the vicinity of the π point of the TM_{01}-like mode. The corresponding FFT spectra of the electric field component as functions of time and space show that only a single frequency is observed. The operation frequency is about 36.27 GHz which is in good agreement with that of the intersection of the dispersion curve with the line of the slow space-charge wave generated on the electron beam. The results of the PIC simulation demonstrate that Cherenkov devices with PBG SWS have good mode selectivity. The phenomenon of cyclotron absorption is also observed and it will be helpful for future experiments.

References

[1] Abe D K, Carmel Y, Miller S M, Bromborsky A, Levush B, Antonsen T M and Destler W W 1998 *IEEE Trans. Plasma Sci.* **26** 591

[2] Main W, Carmel Y, Oyura K, Weaver J, Nusinovich G S, Kobayashi S, Tate J P, Rodgers J, Bromborsky A, Watanabe S, Amin M R, Minami K, Destler W W and Granatstein V L 1994 *IEEE Trans. Plasma Sci.* **22** 566

[3] Alexander N V, Anatoly G S, John C R, Carmel Y, Antonsen T M, Abuelfadl T M, Duan L Z, Vladimir A C, Gregory S N, Botton M and Granatstein V L 2000 *IEEE Trans. Plasma Sci.* **28** 550

[4] Zhang J and Zhong H H 2005 *Acta Phys. Sin.* **54** 206 (in Chinese)

[5] Smirnova E I, Kesar A S, Mastovsky I, Shapiro M A and Temkin R J 2005 *Phys. Rev. Lett.* **95** 074801

[6] Sirigiri J R, Kreischer K E, Machuzak J, Mastovsky I, Shapiro M A and Temkin R J 2001 *Phys. Rev. Lett.* **86** 5628

[7] Han S T, Jeon S G, Shin Y M, Jang K H, Jin K S, Kim J H, Chang S S and Park G S 2005 *IEEE Tran. Plasma Sci.* **33** 679

[8] Bailey A G, Smirnova E I, Earley L M and Carlsten B E 2005 *Proc. SPIE* **6120** 612004

[9] Yin H R, Gong Y B, Wei Y Y, Gong H R, Yue L N, Lu Z G, Huang M Z and Wang W X 2007 *Chin. Phys.* **16** 2737

[10] Chen B, Qian B L and Zhong H H 2006 *High Power Laser and Particle Beams* **18** 862 (in Chinese)

[11] Liu X L, Lei H, Yu T, Feng J J and Liao F J 2007 *Optics Commun.* **281** 102

[12] Gao X, Yang Z Q, Xu Y, Qi L M, Li D Z, Shi Z J, Lan F and Liang Z 2008 *Nucl. Instru. Meth. Phys. Research* A **592** 292

[13] Marsh R A, Shapiro M A and Temkin R J 2007 *Proceedings of PAC07* (Albuquerque: New Mexico, USA) 3005

[14] Di J, Zhu D J, Liu S G 2005 *Journal of University of Electronic Science and Technology of China* **34** 485 (in Chinese)

[15] Miller S M, Antonsen T M, Levush B and Vlasov A N 1996 *IEEE Tran. Plasma Sci.* **24** 859

[16] Goebel D M, Adler E A, Ponti E S, Feicht J R, Eisenhart R L and Lemke R W 1999 *IEEE Tran. Plasma Sci.* **27** 800

[17] Wang H Y, Liang Z and Yang Z Q 2005 *Nucl. Instr. Meth. Phys. Research* A **539** 37